Available online at www.sciencedirect.com

ScienceDirect

Procedia Engineering 181 (2017) 912 – 919

Procedia Engineering

www.elsevier.com/locate/procedia

10th International Conference Interdisciplinarity in Engineering, INTER-ENG 2016

Performance Assessment of ANN in Estimating Remotely Sensed Extracted Bathymetry. Case Study: Eastern Harbor of Alexandria

Omar Makboul[a], Abdelazim Negm[b,*], Saleh Mesbah[a], Mohamed Mohasseb[a]

[a] *Arab Academy for Science, Technology and Maritime Transport, Alexandria-21913, Egypt*
[b] *Water and Water Structures Engineering Dept., Faculty of Engineering, Zagazig University, Zagazig 44519, Egypt*

Abstract

The water depth extraction of shallow water plays an important role for marine safety. It is considered a useful reconnaissance tool to save time and cost to be used in preliminary survey. This paper aims to assess the performance of Artificial Neural Networks (ANN) in estimating the bathymetry of the Eastern harbor of Alexandria Egypt as a case study. This area of the case study represents a low turbid, mud bottom and shallow water area. The estimation of shallow water depth is based on ANN fitting algorithms using the logarithms of multispectral bands reflectance value. The estimation of water depths using optical bands of Landsat-8 multispectral images is extracted directly without regard to other environmental factors (bottom type and sea sediments).The images are first corrected for the effects caused by atmospheric conditions and sun specular. The bands are then calibrated using reference measurements obtained using GPS and single beam echo sounder in the study area. The estimated depths using ANN based on bands 1 &3, 3 only and 2 &3 show higher correlations and lower root mean square error compared the estimation made by previously developed statistically equations which were updated using the same data sets used in developing the ANNs. The ANN has a better capability to estimate the bathymetry using remotely-sensed data extracted from Landsat-8 images.

Peer-review under responsibility of the organizing committee of INTER-ENG 2016

Keywords: Bathymetry; Harbor; Landsat-8; Artificial Neural Network; Hydrographic chart; Remote Sensing.

* Corresponding author. Tel.: +20-100-573-5345; fax: +20-55-2304987.
E-mail address: amnegm85@yahoo.com, amnegm@zu.edu.eg

Peer-review under responsibility of the organizing committee of INTER-ENG 2016
doi:10.1016/j.proeng.2017.02.486

1. Introduction

Bathymetry data is important in many applications such as costal, marine planning and management, and marine safety [1]. Production of bathymetric maps in order to be used in navigation purposes requires accurate water depth. The traditional method for measuring water depth uses shipboard with single or multi beam echo which can measure water depth up to 500m [2] with full bottom coverage and depth accuracy with about 1cm. The density of depth data from echo sounders is limited by the distance *d* between cruise tracks for single beam echo sounders, and by the ratio of depth *h* to *d* (*h/d*) [3]. Moreover, ship-borne surveys are time consuming and relatively expensive. The satellite remote sensing technology has been used for clear water bathymetry mapping providing an easy access and cost-effective way to bathymetry mapping especially for the fast-changing coastal environment studies [4]. The shallow water depth inversion using multispectral remote sensing image has been developed from qualitative analysis to quantitative calculation. Derivate bathymetry from optical sensing is based on the principle that the total amount of radiative energy reflected from a water column is a function of water depth. The theory behind all bathymetric mapping using optical remote sensing is that different wavelengths of light will penetrate water with varying degrees. When the light passes through water it becomes attenuated by interaction with water column according to Beers law Eq 1.

$$l(z) = l(0)exp(-kz) \tag{1}$$

Where, k is the attenuation coefficient, z is the depth and $l(0)$ is the light intensity just below sea surface. The analytical techniques which applied to obtain water depths are optical modeling through establishing a statistical relationship between image pixel values and reference measurements data. The most popular approach was proposed by [5, 6, 7] which assumed that light attenuation is an exponential function of depth and the water quality has no variance within the image area. So, a linear relationship can be derived from the Lambert-Beer law after correcting the specular affects using near infra-red band (NIR) and removal of water column affect for single and pair wavelength bands. Stumpf proposed a ratio algorithm method which uses two or more bands to determine the depth of water based on the difference in attenuation properties between bands [8]. However, the accuracy of the estimated water depths is limited by the attenuation and reflectance characteristics [9]. Likewise, the accuracy of the retrieved water depth is subject to the influence of the sensing environments (solar elevation and azimuth, platform height), water surface conditions (roughness, waves and currents), and atmospheric absorption and scattering [10].

Recently [11] evaluated the use of different statistical models (Principal component analysis, Ratio model and 3rd order polynomial) for extracting depth from Landsat-8 multispectral images in the Eastern harbor of Alexandria. The results showed that the green band is more significant than coastal and blue bands. The contribution of the red band in water depths modeling was not significant [11]. The results showed that ratio model has the form of Eq 2.

$$Z = 2.691 * \frac{ln(R_c)}{ln(R_G)} + 2.985 \tag{2}$$

Where R_c and R_G are, respectively, reflectance of coastal and green bands. And third order polynomial model with the form Eq 3.

$$Z = 27.8 * {R_G}^3 - 43.92 * {R_G}^2 + 12.9 * R_G + 8.25 \tag{3}$$

The third model has the following form of Eq 4.

$$Z = -6.861 * p_1 + 20.47 \tag{4}$$

Where p_1 is factor 1 from principal components. Equations (3) and (2) provided more accurate estimation of the depth compared to Eq. (4). The R^2 and the root mean square error (RMSE) for the three equations are (0.66, 0.74), (0.55, 0.79), and (0.41, 1.5) respectively.

On the other hand, the ANN algorithms were used for bathymetry detection by many researchers [12, 13] and [14]. They used ANN for detecting the nonlinear relationship between reflectance from different spectral bands and water depth. This paper aims to assess the performance of ANN in estimating the bathymetry of the Eastern harbor of Alexandria Egypt using the extracted data of different bands 1, 2 and 3 of Landsat-8 multispectral bands reflectance values as inputs and the reference measurements as a single output.

2. Study area and data collection

2.1. Study area

The study area is the eastern harbor located in North West of Alexandria as shown in Fig 1. The study area of interest is located between the coordinates (31° 12.6' N, 29° 52.9' E), (31° 12.0'N, 29° 53.4' E), (31° 12.4' N, 29° 45.3' E), (31° 12.8' N, 29° 53.9' E), UTM zones 35.It is a portion of the commercial port of Alexandria**.** The harbor is formed by two converging breakwater. The Eastern harbor is shallow and is not navigable by the large-decked ships. However, it is used mainly for fishing boats and yachts.

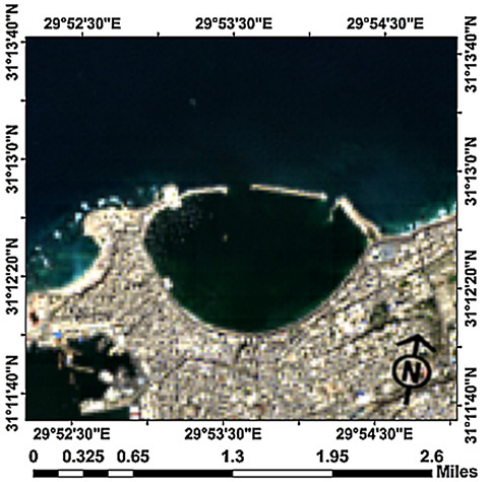

Fig. 1. Landsat-8 image of the study area: eastern harbor of Alexandria [11]

2.2. Data collection

The reference measurements acquisition systems consisted of laptop computers running HYPACK software hydrographic survey software. Devices used in this operation include single-beam echo sounders (NAVI SOUND 210), Trimble 2000 GPS and side scan sonar (Starfish SSS). The weather condition during the period of measurements (from 08.00 to 17.00) was clear in the morning, then partly cloudy and windy. Temperature ranged from 30° C to 31° C breezy. Wind direction was NNE with a speed of 15 to 30 km/h. The echo sounders and DGPS were interfaced to the survey computers via RS-232 serial communication port. The echo sounder transducers were mounted to the rails of the survey vessels amidships and the GPS antenna was mounted directly over the transducer. The region of survey is divided into lines with a total of 20 planed line and 2 cross check lines according to IHO standard order (1a) as shown in Table. 1. The density of reference data was about 2500 measurements of depth. The water depth blow 10m represents 97% of the total area. The average water depth in this area was 4.1mand sea bottom nature is mud. The depth soundings were corrected to chart datum (CD) by subtracting the local tidal height as predicted by Total Tide Software HYPACK software.

The parameters “a” and “b” for each order, as given in Table 1, together with the depth “d” have to be introduced into the Eq 5 in order to calculate the maximum allowable total vertical uncertainty (TVU) for a specific depth.

$$\pm\sqrt{a^2 + (b * d)^2} \quad (5)$$

Where, a represents that portion of the uncertainty that does not vary with depth, b is a coefficient which represents that portion of the uncertainty that varies with depth, d is depth of water and b ∗ d represents the portion of the uncertainty that varies with depth.

Table 1. Summary of Minimum Standards for Hydrographic Surveys order (1) International Hydrographic Bureau (2008)

Examples of typical areas	Harbors, harbor approach channels, recommended tracks and some coastal areas with depths up to 100 m
Horizontal accuracy (95% confidence level)	5 m + 5% of depth
Depth accuracy for reduced depths (95% confidence level)	a = 0.5 m b = 0.013
100% Bottom search	Required in selected areas
System detection capability	Cubic features > 2 m in depths up to 40 m; 10% of depth beyond 40 m
Maximum Line Spacing	3 x average depth or 25 m, whichever is greater

2.3. Sensor data

Landsat-8collects image data for 11 spectral bands with a 30 m spatial resolution. The bands used for detecting bathymetry in this study were costal/ aerosol (0.435-0.451 μm), blue (0.452-0.512 μm), green (0.533-0.590 μm), red (0.636-0.673 μm) and near infrared (NIR) (0.851-0.879 μm).

3. Method

3.1. Artificial Neural Network Model

The basics of ANN can be found in [13-18]. The training procedure of the ANN that presented in [13] was used in this paper till the optimal ANN was obtained by trial and error. The ANN toolbox of MATLAB was used. The correlation coefficient, R, and root mean square, RMSE, were computed for each run during the optimization process of each of the ANN parameters (number of hidden layers, number of neuron in each layer, activation function and learning algorithm), The procedure of building the optimal network is presented in section 4.

3.2. Imagery data pre-processing

Satellite image is affected by a variety of environmental factors such as atmosphere and sun specular. It needs pre-corrections to avoid influencing the inversion depth. The pre-processing has great effect on improving the precision of inversion depth.

3.2.1. Converting to radiance

Convert the digital number (DN) to the spectral radiance at the aperture (L_λ) is measured in ($watts/meter\ squared * ster * \mu m$) using Eq 10.

$$L_\lambda = ML * Qcal + AL \quad (10)$$

Where, ML is Band-specific multiplicative rescaling factor from Land-sat metadata files, Qcal is calibrated standard product pixel values (DN) and AL is Band-specific additive rescaling factor from Land-sat metadata file.

3.2.2. Applying atmospheric correction

The solar radiation passes through the atmosphere before collected by the sensor. Therefore images affected by several factor such as water vapor, distribution of aerosols and visibility [19]. In this paper, the FLASSH model in ENVI software is used to correct the atmospheric effect that applied to the solar wavelength according to Eq 11.

$$L = \left(\frac{A\rho}{1-\rho_e{}^s}\right) + \left(\frac{B\rho_e}{1-\rho_e{}^s}\right) + L_a \quad (11)$$

Where,ρ is the Pixel surface reflectance, $\rho_e$is an average surface reflectance for the pixel and a surrounding region, s is the spherical albedo of the atmosphere and L_a is the radiance back scattered by the atmosphere.

A and B are coefficients that depend on atmospheric and geometric conditions but not on the surface. Moreover, A, B, S and L_a are depending on water vapor amount. This is used in MODTRAN model using calculations that use the viewing and solar angle and the mean surface elevation measurement. The input image for FLAASH module in ENVI software must be a radio-metrically calibrated radiance image and data must be in floating-point format [20]**.**

3.2.3. Applying sun glint correction

Specular reflection of solar radiation, known as sun glint must be removed for accurate benthic habitat classification. Hochberg provided a method to remove sun glint by using the brightness of near-infrared NIR band [21]. Hedley proposed revised method depending on Hochberg assumption that based on the linear relationship between NIR and visible bands using linear regression [22]. By using linear regression of NIR brightness (x-axis) against the visible band brightness (y-axis), this would be homogeneous if not for the presence of sun glint (deep water). The slope of the regression is then used to predict the brightness in the visible band by using Eq 12. This method is not necessary to mask out land or cloud pixels. The minimum sample size required is two pixels

$$R_i' = R_i - b_i(R_{NIR} - MIN_{NIR}) \quad (12)$$

Where,R_i' is the sun-glint corrected pixel brightness in bandi, b_i is the product of regression slope,R_{NIR} is corresponding pixel value in NIR band and MIN_{NIR} is the min NIR value existing in the sample.

4. Results of Building the ANN models and Updating the Statistical Model

Based on the above explained methodology, three networks are developed. All the developed networks used the log-sigmoid activation function in the computations. In building each network, 70% (1750 observations) of the data were used, 15% (375 Observations) for validation and 15% (375 Observations) for testing the performance of the network. The Neural Networks were determined after many experiments with trial and error so that the numbers of nodes and layers as well as the RMSE between calculated and measured depths would be a minimum. The first network (ANN1) used the ratio between bands 1 to 3 as in the input layer with one hidden layers with 5 neurons and the output layer had only one neuron. The training was stopped at 17 iterations with R^2 of test data 0.691 and RMSE of 0.884.

The second network (ANN2) used only band 3 in the input layer with one hidden layers with 10 neurons and the output layer had only one neuron. The resulting R^2 for test data set was 0.699 and RMSE was 0.814. These results were obtained after 18 iterations. The third network (ANN3) used bands 2 and 3 in the input layer with one hidden layers with 15 neurons and the output layer had only one neuron. The value of R^2 for test data was 0.697 while the RMSE for the test data set was 0.876. The training of the network was stopped after 72 iterations. Table 2 summarizes the results of the statistical measures, R^2 and RMSE for the three developed AANs for the three sets of data used to develop the networks.

On the other hand, the previously developed Eq 2, 3 and 4 using bands 1&3, 3 only and 2&3 respectively are updated using the same sets of data used for the training data of the developed networks. The training data of the network was used to estimate the coefficients of the equations while the test data set was used to measure the performance of the updated equations. The updated equations are presented in Eq. 13, 14 and 15 as shown below with the statistical measures, R^2 and RMSE shown in table2.

$$z = 2.242 * \frac{ln(R_C)}{ln(R_G)} + 3.782 \quad (13)$$

$$Z = \ 0.0348 * R_G^3 - 3.005 * R_G^2 - 4.572 * R_G + 10.34 \quad (14)$$

$$z = -3.79 * p1 + 14.58 \quad (15)$$

Table 2. Statistical measures of the developed ANNs and the updated statistical Eq 13, 14 and 15 for each data set.

Statistical model	Band	R2			RMSE		
		Training	Valid.	Testing	Training	Valid.	Testing
ANN1 1-5-1	1,3	0.627	0.601	0.691	0.956	0.998	0.884
Eq.(13)	1,3	0.467	-	0.474	1.154	-	0.779
ANN2 1-10-1	3	0.678	0.647	0.699	0.900	0.936	0.814
Eq.(14)	3	0.613	-	0.609	0.98	-	0.672
ANN3 2-15-1	2,3	0.685	0.712	0.697	0.877	0.853	0.876
Eq.(15)	2,3	0.35	-	0.088	1.253	-	0.64

5. Discussions

Figures 2, 3 and 4 present the comparison between the performance of Eqs. 13-15 and the ANNs. One can observe that the performance of ANNs in predicting the depths is better than the prediction of Eqs. 13-15. In particular, the estimation of ANNs using bands 2 and 3 shows higher performance in terms of R^2 and RMSE (0.697 and 0.876 m) while the performance of the corresponding statistical model using bands 2 and 3 (PCA method) is the lowest in R^2 and RMSE (0.088 and 0.64 m) for the test data set. However, for the training data set, the ANN shows higher performance than the Eq 15 regarding both R^2 and RMSE. The RMSE for ANN in this case is 0.877m while for Eq. 15, it is 1.253m. On the other hand, it is observed that the performance of both ANN and Eq. 14 in the prediction of depths using the green band only (band 3) is higher than using the bands 1 & 3. However, the performance of ANN using bands 1 & 3 for the test data set is higher than that of Eq 13 for the same data set. The value of R^2 is 0.691 for ANN while it is 0.474 for Eq 13 inspire of the RMSE for ANN is 0.884 m and 0.779 m for Eq 13. The training of ANN shows higher performance compared to the training of Eq 13 where R^2 and RMSE are (0.627 and 0.956 m) for ANN and (0.467 and 1.154 m) for Eq 13.

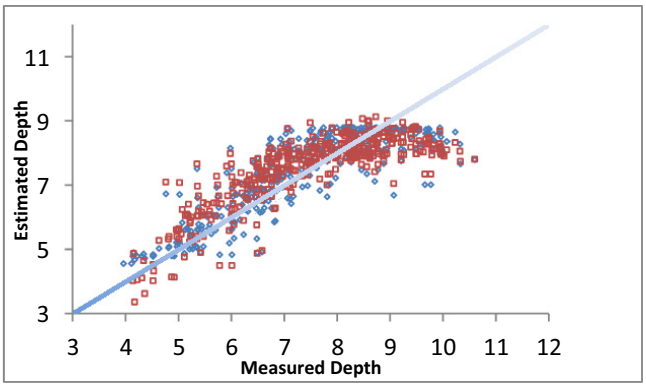

Fig. 2. Measured depth versus estimated depth based on bands 1, 3 using ANN (blue) and the updated Eq no. 13 (red square).

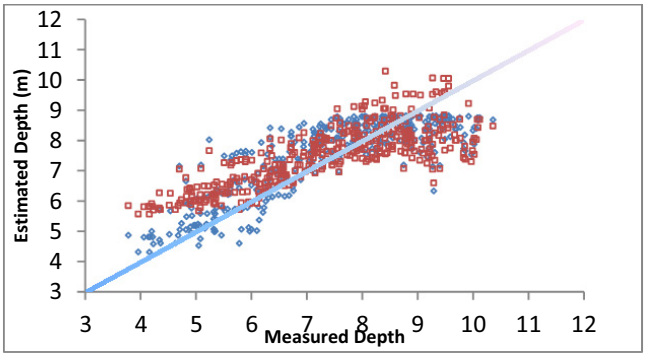

Fig. 3. Measured depth versus estimated depth based on band 3 using ANN (blue) and the updated Eq no. 14 (red square).

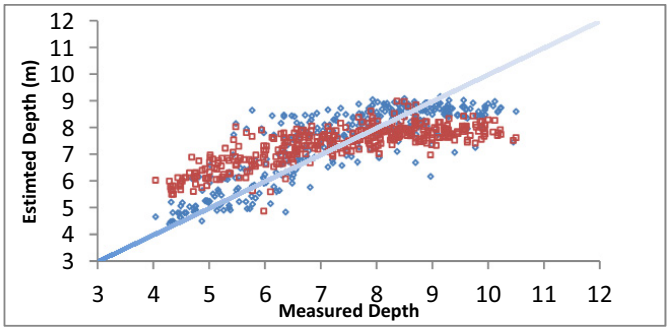

Fig. 4. Measured depth versus estimated depth based on bands 2, 3 using ANN (blue) and the updated Eq no. 15 (red square).

These observations are supported by the data scattering presented in Figures 2, 3 and 4. Eq 15 shows wide scatter compared to the scatter of tested data generated from the ANN with bands 2 and 3 on the input layer. Other cases show more or less similar scatter as the values of R^2 are closer compared to the difference between R^2 of Eq 15 and both other equations and ANNs.

6. Conclusion

The results of this paper indicated that in general the use of the ANNs in estimating the bathymetry of the Eastern harbor of Alexandria Egypt based on the extracted remotely sensed. The use of the green band (band 3) in statistical modeling is superior compared to other developed model while the uses of the blue and green bands (2 and 3) are superior when used with in the ANN. The use of bands 2 and 3 in the statistical modeling is the worst compared to other used bands (3) and (1 & 3).

References

[1] E. P. Green, P. J. Mumby, Edwards A.J, and C. . Clark, Remote Sensing Handbook Tropical Coastal Management, Coastal Management Sourcebook 3, UNESCO, Paris, 2000.

[2] H. Su, H. Liu, and W. D. Heyman, Automated Derivation of Bathymetric Information from Multi-Spectral Satellite Imagery Using a Non-Linear Inversion Model, Mar. Geod. 31 (2008) , 281–298.

[3] C. Liu and L.-G. Leu, Determination of Coral Depth with Formosat-2 Multispectral Image, The 3rd APEC Workshop of SAKE, (2014) , 1–12.

[4] J. S. Ehses and J. J. Rooney, Depth Derivation Using Multispectral WorldView-2 Satellite Imagery, in US Dep. Commer., NOAA Tech , Civ. Environ. Eng. (2015), 24-46.

[5] D. R. Lyzenga, passive remote sensing techniques for mapping water depth and bottom features, Appl. Opt. 17 (1978) , 379–383.

[6] D. R. Lyzenga, Remote sensing of bottom reflectance and water attenuation parameters in shallow water using aircraft and Landsat data, Int. J. Remote Sens. 2 (1981), 71–82.
[7] D. R. Lyzenga, Shallow-water bathymetry using combined lidar and passive multispectral scanner data, Int. J. Remote Sens 6 (1985), 115–125.
[8] R. P. Stumpf, K. Holderied, and M. Sinclair, Determination of water depth with high-resolution satellite imagery over variable bottom types, Limonology Oceanogr 48 (2003), 547–556.
[9] W. D. Philpot, Bathymetric mapping with passive multispectral imagery, Appl. Opt., 28 (1989), 1569–1578.
[10] J. Gao, Bathymetric mapping by means of remote sensing: methods, accuracy and limitations, Prog. Phys. Geogr, 33 (2009), 103–116.
[11] O. Makboul, A. Negm, S. Mesbah, and M. Mohasseb, Assesement of different bathymetre statistical models using LANDSAT-8 multispectral images, in International Conference on Water, Environment, Energy and Society, India, 2016
[12] Z. Zhang and H. Teng, An Inversion Method of Remote Sensing Water Depth Based on Transmission Bands Ratio, in 2011 Fourth International Joint Conference on Computational Sciences and Optimization, IEEE Computer Society , China , 2011, 1002–1006.
[13] H. Mohamed, A. Negm, M. Zahran, and O. C. Saavedra, Assessment of Artificial Neural Network for bathymetry estimation using High Resolution Satellite imagery in Shallow Lakes : Case Study El Burullus Lake , in International Water Technology Conference, Egypt, 2015, 434–444.
[14] W. Yanjiao, Z. Peiqun, D. Wenjie, and Z. Ying, Study on Remote Sensing of Water Depths Based on BP Artificial Neural Network, Mar. Sci. Bull, 9 (2007), 26–35.
[15] D. Graupe, Principles of Artificial Neural Networks (3rd Edtion), World Scientific Publishing Co. Pte. Ltd , Singapore, 2013.
[16] J. M. Walker, Artificial Neural Networks Second Edition, Springer, New York, 2015.
[17] Ö. Ceyhun and A. Yalçın, Remote sensing of water depths in shallow waters via artificial neural networks, Estuar. Coast. Shelf Sci., 89 (2010), 89–96.
[18] M. W. Gardner and S. R. Dorling, Artificial neural networks (the multilayer perceptron) - a review of applications in the atmospheric sciences, Atmos. Environ., 32 (1998), 2627–2636.
[19]C. Song, C. E. Woodcock, K. C. Seto, M. P. Lenney, and S. a. Macomber, Classification and change detection using Landsat TM data: When and how to correct atmospheric effects?, Remote Sens. Environ., 75 (2001), 230–244.
[20] ENVI, ENVI Atmospheric Correction Module: QUAC and FLAASH User's Guide, ITT Visual Information Solutions, 2009.
[21] E. J. Hochberg, S. Andréfouët, and M. R. Tyler, Sea surface correction of high spatial resolution ikonos images to improve bottom mapping in near-shore environments, IEEE Trans. Geosci. Remote Sens, 41 (2003), 1724–1729.
[22] J. D. Hedley, a. R. Harborne, and P. J. Mumby, Technical note: Simple and robust removal of sun glint for mapping shallow water benthos, Int. J. Remote Sens, 26 (2005), 2107–2112.